

PMSTPCOL PEmails

From: Govan, Tekia
Sent: Tuesday, March 23, 2010 3:38 PM
To: Scott Head
Cc: STPCOL
Subject: Article in the Bulletin of the Seismological Society of America Journal
Attachments: ChuckMueller.pdf

Tekia V. Govan, Project Manager
U.S. Nuclear Regulatory Commission
Office of New Reactors
MS T-6-D48
Washington DC 20555-0001
301-415-6197
Tekia.Govan@nrc.gov

Hearing Identifier: SouthTexas34Public_EX
Email Number: 2041

Mail Envelope Properties (F5A4366DF596BF458646C9D433EA37D728FFD16F9B)

Subject: Article in the Bulletin of the Seismological Society of America Journal
Sent Date: 3/23/2010 3:38:16 PM
Received Date: 3/23/2010 3:38:18 PM
From: Govan, Tekia

Created By: Tekia.Govan@nrc.gov

Recipients:
"STPCOL" <STP.COL@nrc.gov>
Tracking Status: None
"Scott Head" <smhead@stpegs.com>
Tracking Status: None

Post Office: HQCLSTR01.nrc.gov

Files	Size	Date & Time
MESSAGE	231	3/23/2010 3:38:18 PM
ChuckMueller.pdf	1895956	

Options
Priority: Standard
Return Notification: No
Reply Requested: No
Sensitivity: Normal
Expiration Date:
Recipients Received:

The Influence of Maximum Magnitude on Seismic-Hazard Estimates in the Central and Eastern United States

by Charles S. Mueller

Abstract I analyze the sensitivity of seismic-hazard estimates in the central and eastern United States (CEUS) to maximum magnitude (m_{\max}) by exercising the U.S. Geological Survey (USGS) probabilistic hazard model with several m_{\max} alternatives. Seismicity-based sources control the hazard in most of the CEUS, but data seldom provide an objective basis for estimating m_{\max} . The USGS uses preferred m_{\max} values of moment magnitude 7.0 and 7.5 for the CEUS craton and extended margin, respectively, derived from data in stable continental regions worldwide. Other approaches, for example analysis of local seismicity or judgment about a source's seismogenic potential, often lead to much smaller m_{\max} .

Alternative models span the m_{\max} ranges from the 1980s Electric Power Research Institute/Seismicity Owners Group (EPRI/SOG) analysis. Results are presented as hazard ratios relative to the USGS national seismic hazard maps. One alternative model specifies m_{\max} equal to moment magnitude 5.0 and 5.5 for the craton and margin, respectively, similar to EPRI/SOG for some sources. For 2% probability of exceedance in 50 years (about 0.0004 annual probability), the strong m_{\max} truncation produces hazard ratios equal to 0.35–0.60 for 0.2-sec spectral acceleration, and 0.15–0.35 for 1.0-sec spectral acceleration. Hazard-controlling earthquakes interact with m_{\max} in complex ways. There is a relatively weak dependence on probability level: hazard ratios increase 0–15% for 0.002 annual exceedance probability and decrease 5–25% for 0.00001 annual exceedance probability. Although differences at some sites are tempered when faults are added, m_{\max} clearly accounts for some of the discrepancies that are seen in comparisons between USGS-based and EPRI/SOG-based hazard results.

Introduction

In most of the central and eastern United States (CEUS; east of the Rocky Mountain front or about longitude -105°), causal relationships between earthquakes and potential seismogenic features are enigmatic. The U.S. Geological Survey (USGS) uses only four specific fault sources in its probabilistic seismic hazard model for the CEUS part of the national seismic hazard maps (Frankel *et al.*, 1996, 2002; Petersen *et al.*, 2008): New Madrid, Charleston, Meers, and Cheraw. In the USGS analysis, historical seismicity (Frankel, 1995) controls the mid- to high-frequency hazard at most CEUS sites. Activity rates are modeled using truncated exponential (Gutenberg–Richter) frequency-magnitude distributions: $N_m = 10^{a-bm}$, where N_m represents the rate of earthquakes with magnitude m , a specifies the overall rate of seismic activity, and b specifies the relative rates of large and small earthquakes. A key parameter that must be specified in any such seismic-hazard calculation is the upper truncation magnitude of the frequency-magnitude distribution for each source, which is the largest possible earthquake (a magnitude that will *never* be ex-

ceeded) given the seismic and tectonic setting, called maximum magnitude or m_{\max} .

In the tectonically active western United States (WUS), the USGS assumes that most structures capable of hosting earthquakes larger than about magnitude 6.5–7.0 are known from their seismicity and/or geology signatures, and several hundred faults are included as specific sources in the WUS hazard model. In such a data-rich region, maximum (or characteristic) magnitudes for faults can be estimated directly from their seismic histories or from empirical correlations with physical parameters like fault length, fault area, or coseismic slip. The USGS uses historical seismicity in the WUS to account for the rest of the hazard, from earthquakes in the magnitude range below m_{\max} 7.0 for most sources.

For most of the CEUS, however, with poor identification of seismogenic structures, low earthquake rates, and seismicity catalogs much shorter in duration than the recurrence times of large earthquakes, earth-science data do not provide an objective, robust basis for estimating m_{\max} for seismicity-based sources, and published estimates vary widely. In the

mid-1980s, the Electric Power Research Institute/Seismicity Owners Group (EPRI/SOG, 1988) conducted a comprehensive, then state-of-the-art seismic-hazard analysis for the CEUS, eliciting hazard models and assessments from six expert earth-science teams. The documentation for that project describes criteria and methods that are still widely used to estimate m_{\max} for data-poor regions, including: (1) magnitude of the largest observed earthquake, with or without an added increment; (2) statistical analysis of the catalog to estimate the sizes and recurrence times of extreme events; (3) judgment based on a potential seismogenic feature's physical dimensions, crustal setting, crustal expression, or the like; (4) extrapolating the frequency-magnitude curve to long recurrence times (for example, the 1000-year earthquake); (5) expanding the local dataset by importing seismicity data from global tectonic/geologic analog regions (substituting space for time); and (6) saturation of the m_b magnitude scale (EPRI/SOG specified m_{\max} in terms of m_b). The teams used combinations of these (and other) methods and also grappled with the problem of assigning defensible weights to distributed m_{\max} values in order to model uncertainty. At the same time, scientists were compiling and analyzing data on earthquakes in stable continental regions worldwide, which are CEUS tectonic analogs, and the

EPRI/SOG teams apparently saw early versions of work by Coppersmith *et al.* (1987) and Johnston (1994). Coppersmith *et al.* (1987) argued that a “significantly higher degree of confidence in the maximum earthquake is possible when placed in the context of the global dataset,” and this notion seems to have influenced some of the teams.

A summary of the myriad EPRI/SOG m_{\max} models is not feasible here, but some generalizations can be attempted. Outside of the few CEUS sources with high rates of seismicity and/or large historical earthquakes, m_{\max} distributions are generally broad, reflecting many different approaches and large uncertainties. Distributions typically range from lower values near the magnitude of the largest historical earthquake to upper values near m_b 6.5–7.5, with upper-range m_{\max} choices tending to favor various combinations of criteria 3–6 listed previously. When weights are considered, distribution centers of mass lie in the mid- m_b -6 range for more active sources and the mid- m_b -5 range for quieter sources, as a rough generalization.

The USGS bases its CEUS m_{\max} choices on the global, stable-continental-region (SCR) seismicity dataset (Coppersmith *et al.*, 1987; Johnston, 1994; Wheeler and Frankel, 2000; Wheeler and Cramer, 2002; Petersen *et al.*, 2008; Wheeler and Johnston, 2008), avoiding judgments based on the inadequate local seismic history or on the seismogenic potential of enigmatic tectonic features that are, at best, only weakly associated with past earthquakes. They divide central and eastern North America into two broad tectonic/geologic zones: the older central craton and the younger rifted (extended-crust) margin, referred to, respectively, as the “Precambrian craton” and “Phanerozoic rim” in Wheeler and Frankel (2000), and as the “craton” and “margin” hereinafter.

Table 1

EPRI/SOG m_{\max} (m_b) for North Anna Site Host Source Zones

Team	Host Source Zone (Team Code)	m_{\max} (Weight)
Bechtel	Central Virginia (E)	5.4 (0.1)
		5.7 (0.4)
		6.0 (0.4)
	S. Appalachians (BZ5)	6.6 (0.1)
		5.7 (0.1)
		6.0 (0.4)
		6.3 (0.4)
		6.6 (0.1)
		6.6 (0.1)
Dames and Moore [*]	S. Cratonic Margin (default zone) (41)	6.1 (0.8)
		7.2 (0.2)
Law	Eastern Basement (17)	5.7 (0.2)
		6.8 (0.8)
	Eastern Basement Background (217)	4.9 (0.5)
		5.7 (0.5)
Rondout	Central VA (29)	6.6 (0.3)
		6.8 (0.6)
		7.0 (0.1)
	Shenandoah (30)	5.2 (0.3)
		6.3 (0.55)
		6.5 (0.15)
Weston	Central VA Seismic Zone (22)	5.4 (0.19)
		6.0 (0.65)
		6.6 (0.16)
	104–25 (C21), 104–26 (C22), backup104–28BE–26 (C34), 104–28BE–25 (C35)	5.4 (0.24)
		6.0 (0.61)
		6.6 (0.15)
Woodward-Clyde	North Anna Background (B22)	5.8 (0.33)
		6.2 (0.34)
		6.6 (0.33)

*For PSHA, Dames and Moore use distributions ± 0.2 magnitude units around these central values, with weights 0.25, 0.5, and 0.25 (EPRI/SOG, 1988).

Table 2

EPRI/SOG m_{\max} (m_b) for the South Texas Project Site Host Source Zones^{*}

Team	Host Source Zone (Team Code)	m_{\max} (Weight)
Bechtel	Gulf Coast (BZ1)	5.4 (0.1)
		5.7 (0.4)
		6.0 (0.4)
		6.6 (0.1)
Dames and Moore [†]	South Coastal Margin (20)	5.3 (0.8)
		7.2 (0.2)
Law	South Coastal Block (126)	4.6 (0.9)
		4.9 (0.1)
Rondout	Gulf Coast to Bahamas Fracture Zone (51)	4.8 (0.2)
		5.5 (0.6)
Weston	Gulf Coast (107)	5.8 (0.2)
		5.4 (0.71)
		6.0 (0.29)
Woodward-Clyde	Central U.S. Background (B43)	4.9 (0.17)
		5.4 (0.28)
		5.8 (0.27)
		6.5 (0.28)

*Not updated, see text.

†For PSHA, Dames and Moore use distributions ± 0.2 magnitude units around these central values, with weights 0.25, 0.5, and 0.25 (EPRI/SOG, 1988).

Overall, the CEUS margin is more seismically active than the craton, and continental margins worldwide have hosted the largest SCR earthquakes. The USGS specifies m_{\max} in terms of moment magnitude. For seismicity-based sources in the CEUS, they use m_{\max} distributions peaked at moment magnitude 7.0 (m_b 6.8–7.0) for the craton and 7.5 (m_b 7.1–7.3) for the margin. The USGS also specifies m_{\max} 7.5 for a zone encompassing large paleoearthquakes near the Wabash Valley (Wheeler and Cramer, 2002); for simplicity hereinafter, “margin” refers to both of the m_{\max} -7.5 regions, the margin (as defined previously), and Wabash.

For geographically comparable seismic sources, the USGS m_{\max} values are generally greater than all but the greatest values in the upper tails of the EPRI/SOG m_{\max} distributions. Since 2003, the USGS has collaborated with the United States Nuclear Regulatory Commission (NRC) to review seismic hazard assessments that are submitted with all applications to build new nuclear power plants in the United States. All applications to date have been for reactor sites located in the CEUS, and, following NRC guidelines, all have been based on the EPRI/SOG analysis (updated to reflect new information)—including the EPRI/SOG m_{\max} specifications. In these reviews, hazard results from the USGS and the applicants are naturally compared, and in many cases the USGS probabilistic ground motions are significantly greater, by factors of two or more at some sites. Although there are other probabilistic seismic hazard analysis (PSHA) modeling differences between the USGS and the NRC applicants, this study focuses on the influence of m_{\max} . I address the problem of m_{\max} sensitivity by exercising the USGS hazard model and computer codes with alternative m_{\max} distributions that sample the ranges specified by the NRC applicants, using the USGS model as a reference. Results are presented as seismic-

hazard maps, hazard ratio maps, and as tables of hazard ratios for 16 selected city sites.

EPRI/SOG and USGS m_{\max} Distributions for Two CEUS Sites

Examples of the EPRI/SOG team m_{\max} distributions for the host source zones for two CEUS nuclear power plant sites are shown in Tables 1 and 2. The North Anna site (Table 1) is located in central Virginia, near the seismically active Central Virginia Seismic Zone. The South Texas Project site (Table 2) lies near the Gulf of Mexico coast, roughly midway between Galveston and Corpus Christi, in a relatively quiet region. Data are taken from the North Anna (Dominion Nuclear North Anna, 2006) and South Texas Project (South Texas Project Nuclear Operating Company, 2008) NRC applications. In each case, the shapes and sizes of the source zones are different for the six teams, the common factor being that each zone hosts the plant site (e.g., Table 1 lists the zones with distance = 0 in tables 2.5–5 to 2.5–10 of the North Anna application). (Some teams specify more than one host zone; neither their probabilities of activity nor any source interdependencies are considered here.) On average, the teams specify greater m_{\max} for the more active North Anna sources (best seen by comparing the tables team by team). For the North Anna sources, EPRI/SOG m_{\max} ranges from m_b 4.9 to 7.2, averaging about m_b 6.1. For the South Texas sources, EPRI/SOG m_{\max} ranges from m_b 4.6 to 7.2, averaging about m_b 5.5. (For the application, NRC required updates to the South Texas m_{\max} distributions, based on two large earthquakes in the Gulf of Mexico in 2006. I show the original values in Table 2 because they are representative of EPRI/SOG m_{\max} choices for some quiet CEUS sources.) Both sites lie within the CEUS margin, so, for both, the USGS

Table 3
USGS Gridded-Seismicity Source Models

Source Model	Adjust Rates for Magnitude Uncertainty?	m_{\max} * (Moment Magnitude)	Moment Magnitude to m_b Conversion †	Weight
1	yes	6.6c7.1m	AB95	0.0167
2	yes	6.8c7.3m	AB95	0.0333
3	yes	7.0c7.5m	AB95	0.0833
4	yes	7.2c7.7m	AB95	0.0333
5	yes	6.6c7.1m	J96	0.0167
6	yes	6.8c7.3m	J96	0.0333
7	yes	7.0c7.5m	J96	0.0833
8	yes	7.2c7.7m	J96	0.0333
9	no	6.6c7.1m	AB95	0.0333
10	no	6.8c7.3m	AB95	0.0667
11	no	7.0c7.5m	AB95	0.1667
12	no	7.2c7.7m	AB95	0.0667
13	no	6.6c7.1m	J96	0.0333
14	no	6.8c7.3m	J96	0.0667
15	no	7.0c7.5m	J96	0.1667
16	no	7.2c7.7m	J96	0.0333

*6.6c7.1m denotes m_{\max} = 6.6 in the craton and 7.1 in the margin, and so on.

†AB95 is Atkinson and Boore (1995); J96 is Johnston (1996).

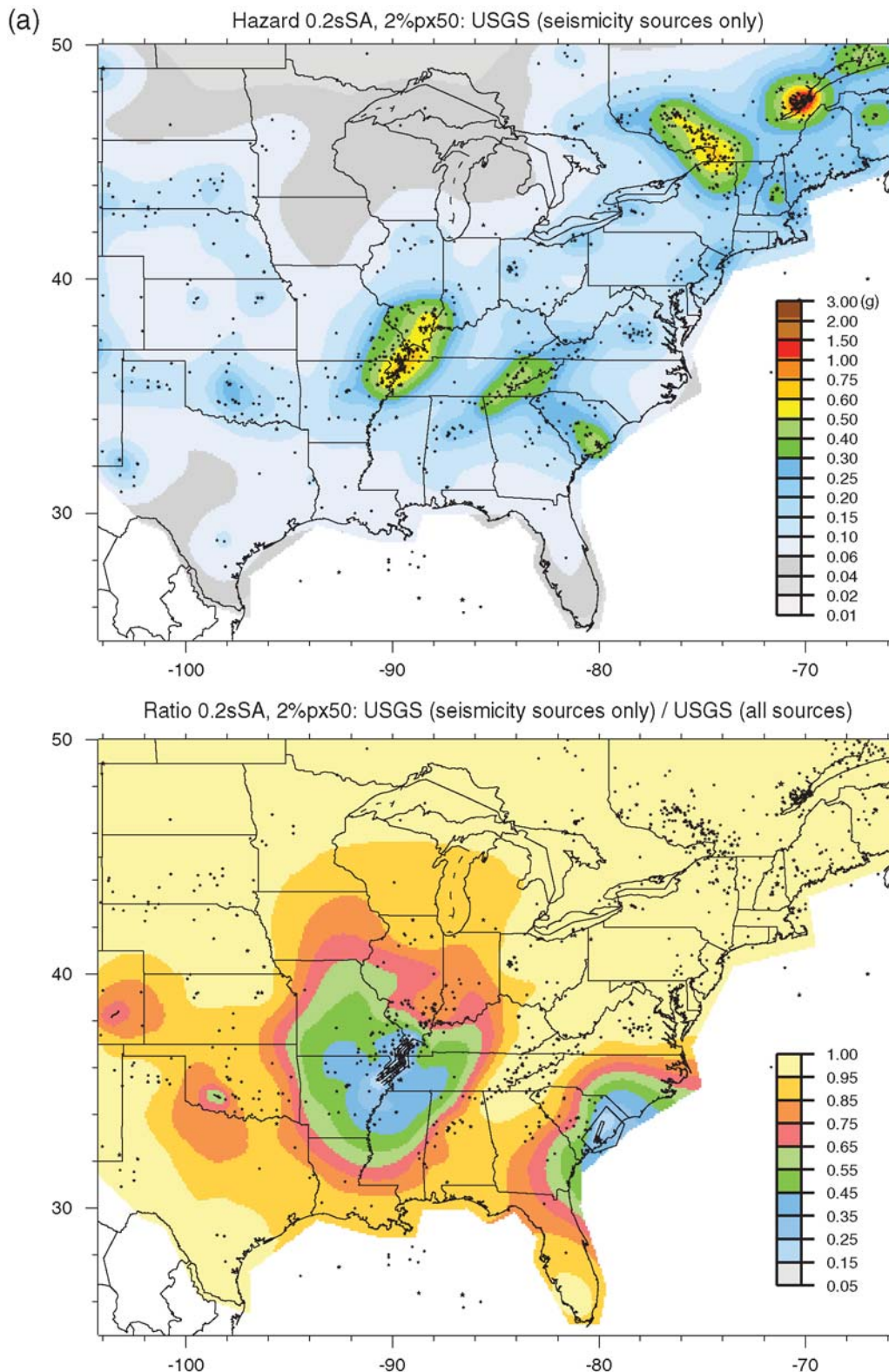
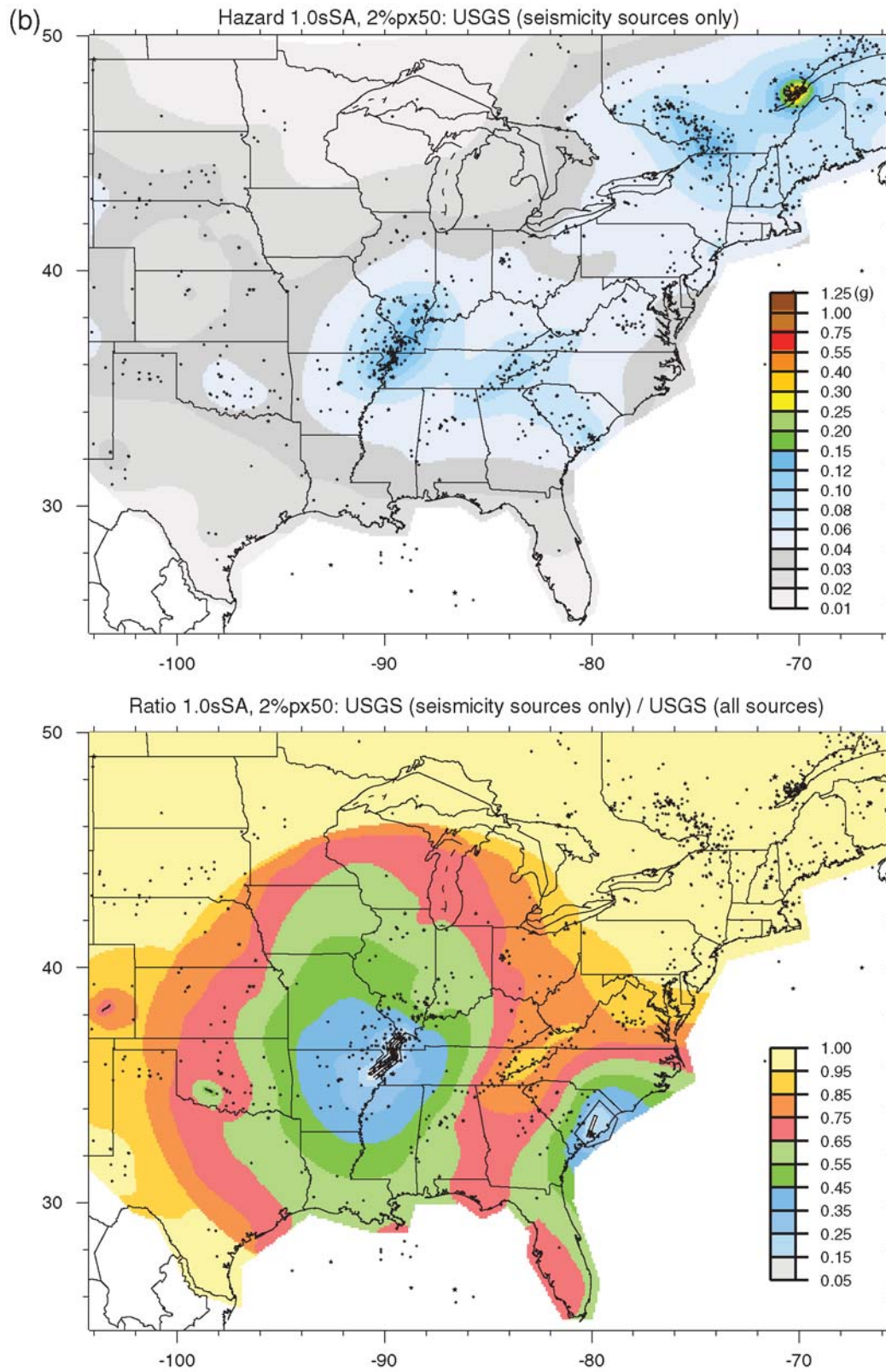


Figure 1. (a) Top: Seismic hazard map for 0.2-sec spectral acceleration (2% probability of exceedance in 50 years) using the USGS hazard model with seismicity sources only. Bottom: Ratio seismic hazard map using the USGS seismicity-sources-only model for the numerator and the USGS all-sources model for the denominator. Warm colors, sites where seismicity-based sources dominate the hazard; black lines in bottom panel, modeled faults (Cheraw in Colorado, Meers in Oklahoma, and five hypothetical New Madrid traces) and fault zones (narrow and broad Charleston zones); black stars, epicenters of modeled earthquakes. See [Frankel *et al.* \(1996, 2002\)](#) and [Petersen *et al.* \(2008\)](#) for PSHA details. (b) Like Figure 1a but for 1.0-sec spectral acceleration. Warm colors in the ratio map (bottom panel), sites where seismicity-based sources dominate the hazard. (Continued)



would specify an m_{\max} distribution peaked at moment magnitude 7.5 (m_b 7.1–7.3) for local sources.

The USGS Seismic Hazard Model for the CEUS

Methodology Details

With few specific faults to model, PSHA practice for the CEUS has generally relied on seismicity-based methods. The USGS uses a gridded-and-smoothed-seismicity approach (an alternative to traditional source zones) that is based on the expectation that future hazardous earthquakes will occur near past small and moderate-size events (Frankel, 1995; Frankel *et al.*, 1996). Rate parameters (local a values and regional b values) and completeness levels are estimated from statistical analysis of a declustered earthquake catalog (e.g., Mueller *et al.*, 1997). For each grid cell (0.1° in latitude and longitude in the national seismic hazard maps), three model rates for earthquakes with m_b equal to or greater than 3, 4, and 5 are computed from the catalog using a maximum-likelihood, variable-completeness method (Weichert, 1980). These three rates are spatially smoothed, then weighted and averaged along with a background rate (accounting for possible future earthquakes in regions with little or no past activity). Each grid cell becomes an individual seismic source in the PSHA calculation; hazard from each cell is computed over a frequency-magnitude distribution that is pinned at the average earthquake rate and truncated at m_{\max} . The USGS maps show mean seismic hazard for a suite of published ground-motion-prediction relations and a (nationally uniform) $V_{530} = 760$ m/sec site condition.

For the 2008 CEUS hazard maps (Petersen *et al.*, 2008), the USGS computes two seismicity rate grids: one with rates adjusted to account for uncertainties in historical earthquake magnitudes (following Felzer, 2008) and one without, combined with respective weights of 0.333 and 0.667. As noted previously, the USGS uses m_{\max} distributions peaked at moment magnitude 7.0 for the craton and 7.5 for the margin. Distributions around each preferred magnitude value, PV , are specified as: $PV-0.4$ with weight 0.1, $PV-0.2$ with weight 0.2, PV with weight 0.5, and $PV+0.2$ with weight 0.2. This is referred to as the reference or USGS m_{\max} model hereinafter. For hazard calculations, moment-magnitude m_{\max} is converted to equivalent m_b using conversion rules published by Atkinson and Boore (1995) and Johnston (1996) with equal weights. The two rate grids, four m_{\max} branches, and two magnitude-conversion rules yield 16 gridded seismicity models, as shown in Table 3. Hazard results are computed for each model and combined using the weights listed in the last column of Table 3.

Hazard from Seismicity Sources Only

To make the final, official USGS hazard maps for the CEUS, hazard curves from the gridded-seismicity sources are combined with hazard curves from the New Madrid, Charleston, Meers, and Cheraw faults at each site. Results for 2%

probability of exceedance in 50 years (2%px50) from the seismicity-sources-only model and the full source model (with the faults) are compared in Figure 1a for 0.2-sec spectral acceleration (0.2sSA) and in Figure 1b for 1.0-sec spectral acceleration (1.0sSA). The top panel in each figure shows the hazard map computed using only the seismicity sources. Each map is divided by the corresponding hazard map computed using the full source model (not shown), and the ratio map is plotted in the bottom panel of each figure. Figure 1a (and a similar result, not shown, for peak ground acceleration, PGA) shows that seismicity sources control the mid- to high-frequency hazard at most sites (away from the faults) in the CEUS. The influence of the faults extends to greater distances for longer structural periods, but the 1.0-sec hazard is still dominated by the seismicity sources at many sites (Fig. 1b).

Analysis

It is particularly important to quantify the influence of m_{\max} for seismicity-based seismic sources in the CEUS, both because these sources control the hazard at many sites and because their m_{\max} choices are especially controversial and poorly constrained by local data. In order to focus on this issue, the faults are excluded for most of the comparisons that follow. The specification of maximum (or characteristic) magnitudes for specific faults is a fundamentally different problem that is outside the scope of this study. Hazard results computed using the standard USGS m_{\max} model with the gridded-seismicity-only source model (Table 3, top panels in Fig. 1) serve as references for most of the m_{\max} sensitivity tests. For example, the map plotted in the top panel of Figure 1a is used as the denominator (reference) when m_{\max} sensitivity for 0.2sSA is expressed as a ratio of hazard maps (using a numerator map developed from an alternative m_{\max} model).

In formulating models for testing, the goal is to sample the range of current, state-of-practice m_{\max} choices with a tractable number of simple alternatives. The EPRI/SOG (1988) teams specified broad, complex m_{\max} distributions, ranging from below m_b 5 to above m_b 7 for many sources (e.g., Tables 1 and 2). Like the USGS, some teams specified greater m_{\max} for sources located in rifted terranes. I use a variation of the USGS approach to construct four alternate m_{\max} models: M5.0c5.5m specifies m_{\max} (moment magnitude) equal to 5.0 for the craton and 5.5 for the margin, and so on for models M6.0c6.5m, M7.0c7.5m, and M7.5c8.0m. These models are listed, along with equivalent m_b values calculated with the Atkinson and Boore (1995) and Johnston

Table 4
Alternative m_{\max} Models for Testing Hazard Sensitivity

m_{\max} Model (Moment Magnitude)	Equivalent m_b (AB95 Conversion)	Equivalent m_b (J96 Conversion)
M5.0c5.5m	5.47c, 5.90m	5.27c, 5.67m
M6.0c6.5m	6.29c, 6.66m	6.04c, 6.40m
M7.0c7.5m	7.00c, 7.32m	6.74c, 7.07m
M7.5c8.0m	7.32c, 7.63m	7.07c, 7.38m

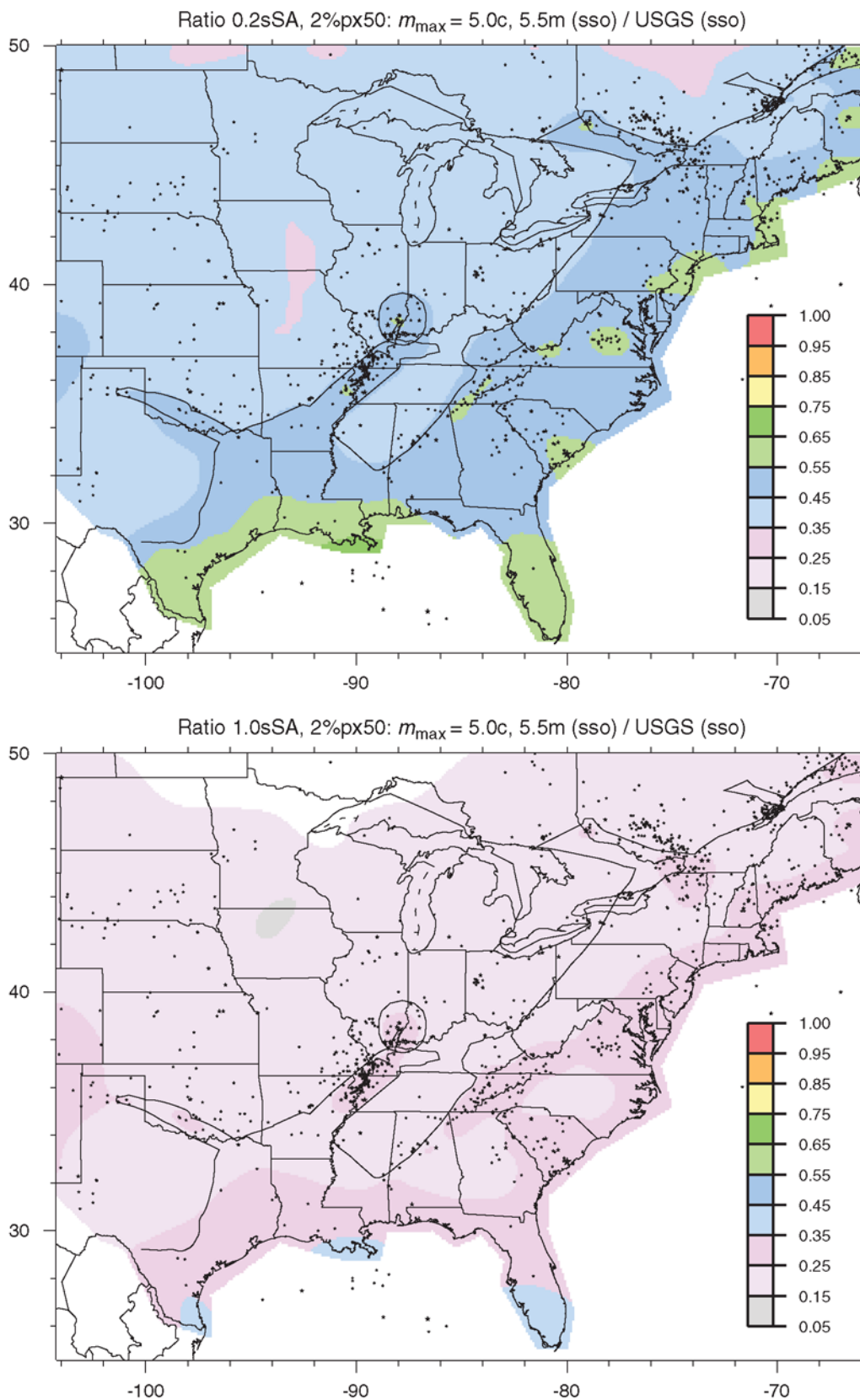


Figure 2. Ratio seismic hazard maps (2% probability of exceedance in 50 years) using alternate m_{max} model M5.0c5.5m for the numerator and USGS reference m_{max} model for the denominator. The strong m_{max} truncation reduces the probabilistic ground motions. Black lines, boundary between the craton and extended-margin m_{max} zones and the outline of the Wabash m_{max} zone; black stars, epicenters of earthquakes used in the hazard calculations. Top: 0.2-sec spectral acceleration. Bottom: 1.0-sec spectral acceleration.

(1996) conversion rules, in Table 4. (The m_b , m_{\max} values listed in Table 4 can be compared directly with the EPRI/SOG values.) Some of the EPRI/SOG teams specified very small m_{\max} for some sources, including some even smaller than m_b , 5.0, the minimum magnitude considered in the hazard calculation (m_{\min}). I recognize that the m_{\max} values used in the smallest- m_{\max} alternate model, M5.0c5.5m, are somewhat greater than the smallest values used by the EPRI/SOG teams. I also note, however, that it becomes increasingly difficult to quantify the influence of m_{\max} on hazard as m_{\max} approaches m_{\min} because at many sites the hazard falls to the floor value specified in the computer code, making ratios meaningless. At any rate, the models tested here come close to spanning the centers of the EPRI/SOG distributions. M7.5c8.0m is included as a model that specifies m_{\max} values slightly greater than both the EPRI/SOG teams and the USGS.

All PSHA parameters except m_{\max} are held fixed. Like the reference model, each alternate calculation combines two seismicity rate grids (with and without magnitude-uncertainty rate adjustments with respective weights of 0.333 and 0.667) and two magnitude-conversion rules (Atkinson and Boore, 1995, and Johnston, 1996, with equal weights). Unlike the reference model, only the central m_{\max} values are used for each alternate. In the figures and tables, the abbreviation USGS denotes the reference m_{\max} model, and the abbreviation sso reminds the reader that seismicity sources only are used. Results are not mapped (maps are blank) at sites where the hazard falls to the floor value specified in the computer code.

Results for 2% Probability of Exceedance in 50 Years

Figure 2 and Table 5 show the primary results for the smallest- m_{\max} alternate model: hazard ratios for 2%px50 using M5.0c5.5m for the numerator and the reference USGS

m_{\max} model for the denominator. For 0.2sSA, the strong m_{\max} truncation in M5.0c5.5m produces hazard ratios equal to 0.35–0.60 at most sites (top panel of Fig. 2; average hazard ratio about 0.46 ± 0.08 for the 16 cities in Table 5). Results (not shown) are similar for PGA. Differences are not uniform spatially, with greater hazard ratios at seismically active sites and sites in the margin and smaller hazard ratios at quiet sites and sites in the craton. Some of these patterns can be explained by considering the complex ways in which modeled earthquakes control the hazard in a PSHA. Probabilistic hazard tends to be dominated by smaller, more local earthquakes at sites in active regions, with control shifting to larger, more distant sources at quieter sites. Greater hazard ratios correlate spatially with clusters of high seismicity because the m_{\max} truncation deletes relatively fewer hazard-controlling earthquakes for these sites. Hazard ratios are generally greater at sites in the margin than in the craton, even though both the alternate and reference models specify a uniform 0.5-magnitude-unit differential between m_{\max} in the craton and margin. The difference, presumably, occurs because the m_{\max} truncation removes relatively more hazard-controlling earthquakes in the mid- m_b -5 range for sources in the craton. Also, because some modeled ground motions saturate for the largest earthquakes, the m_{\max} truncation may remove relatively less hazard in the margin (A. Frankel, personal comm., 2008). Because longer-period hazard tends to be controlled by larger earthquakes, the m_{\max} truncation has an even stronger effect on the 1.0-sec hazard. For 1.0sSA, M5.0c5.5m produces hazard ratios equal to 0.15–0.35 at most sites (bottom panel of Fig. 2; average hazard ratio about 0.24 ± 0.05 for the 16 cities in Table 5).

Results for M6.0c6.5m are presented in Figure 3 and Table 5. The less severe m_{\max} truncation produces hazard ratios equal to 0.70–0.85 for 0.2sSA (top panel of Fig. 3; average hazard ratio about 0.76 ± 0.04 for the 16 cities in

Table 5
Hazard Ratios for 2%px50 (about 0.0004apx): Alternative m_{\max} (sso)/USGS (sso)

	m_{\max} Model					
	M5.0c5.5m		M6.0c6.5m		M7.0c7.5m	
	0.2sSA	1.0sSA	0.2sSA	1.0sSA	0.2sSA	1.0sSA
Boston	0.55	0.29	0.79	0.60	1.01	1.02
New York City	0.57	0.32	0.83	0.64	1.01	1.02
Washington, DC	0.51	0.26	0.77	0.58	1.01	1.02
Pittsburgh	0.45	0.21	0.74	0.53	1.01	1.02
Charleston	0.59	0.34	0.83	0.67	1.01	1.02
Atlanta	0.49	0.24	0.74	0.56	1.02	1.03
Cincinnati	0.38	0.18	0.70	0.51	1.01	1.02
Chicago	0.37	0.18	0.75	0.52	1.01	1.02
Memphis	0.52	0.25	0.78	0.58	1.01	1.02
Baton Rouge	0.57	0.31	0.82	0.61	1.01	1.02
St. Louis	0.38	0.19	0.72	0.53	1.01	1.02
Minneapolis	0.38	0.16	0.74	0.49	1.00	1.01
Wichita	0.37	0.18	0.72	0.51	1.01	1.01
Austin	0.49	0.26	0.78	0.58	1.01	1.02
Rapid City	0.37	0.19	0.72	0.51	1.00	1.01
Denver	0.41	0.25	0.73	0.54	1.00	1.01

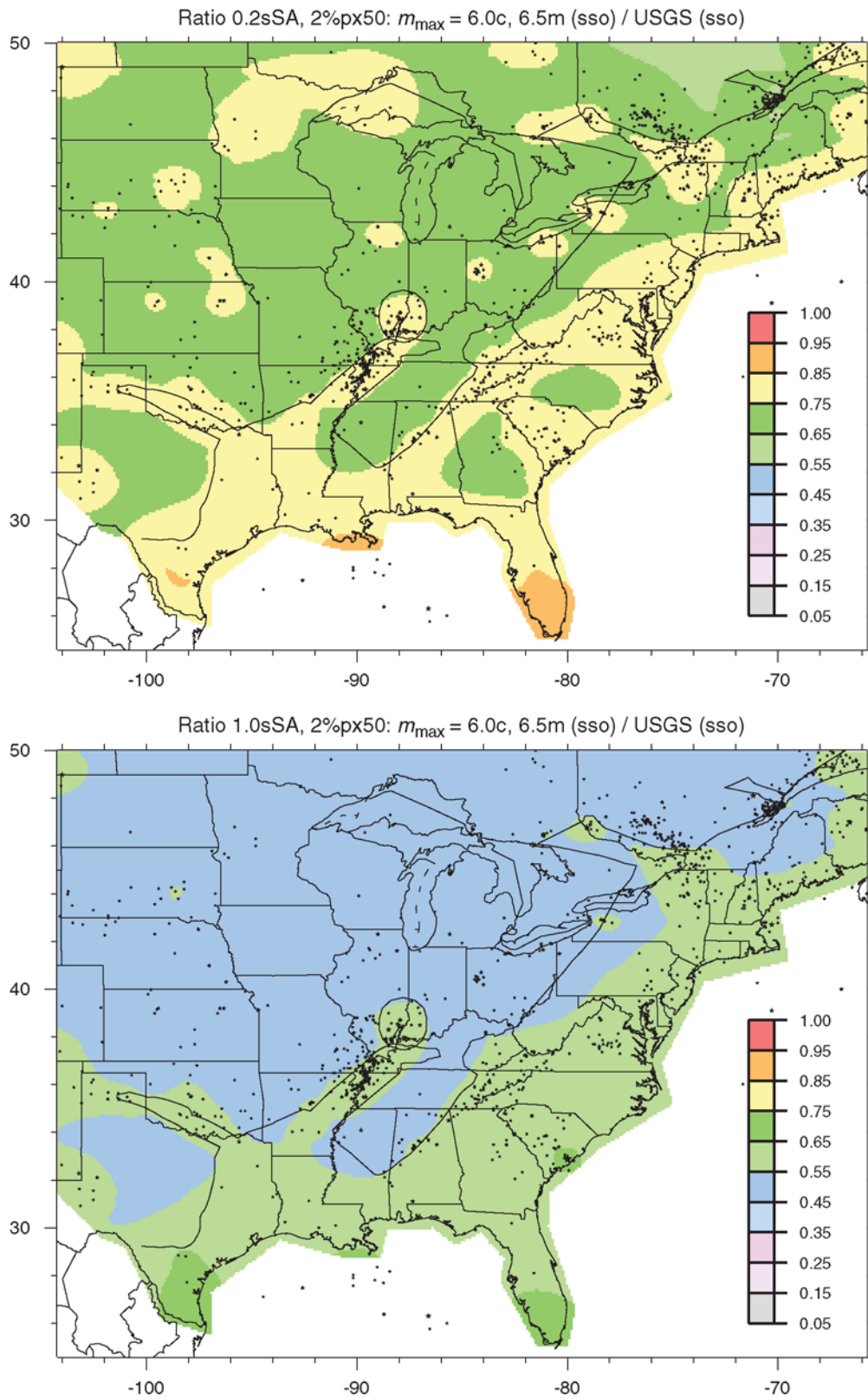


Figure 3. Like Figure 2 but with alternate m_{max} model M6.0c6.5m for numerator (weaker m_{max} truncation).

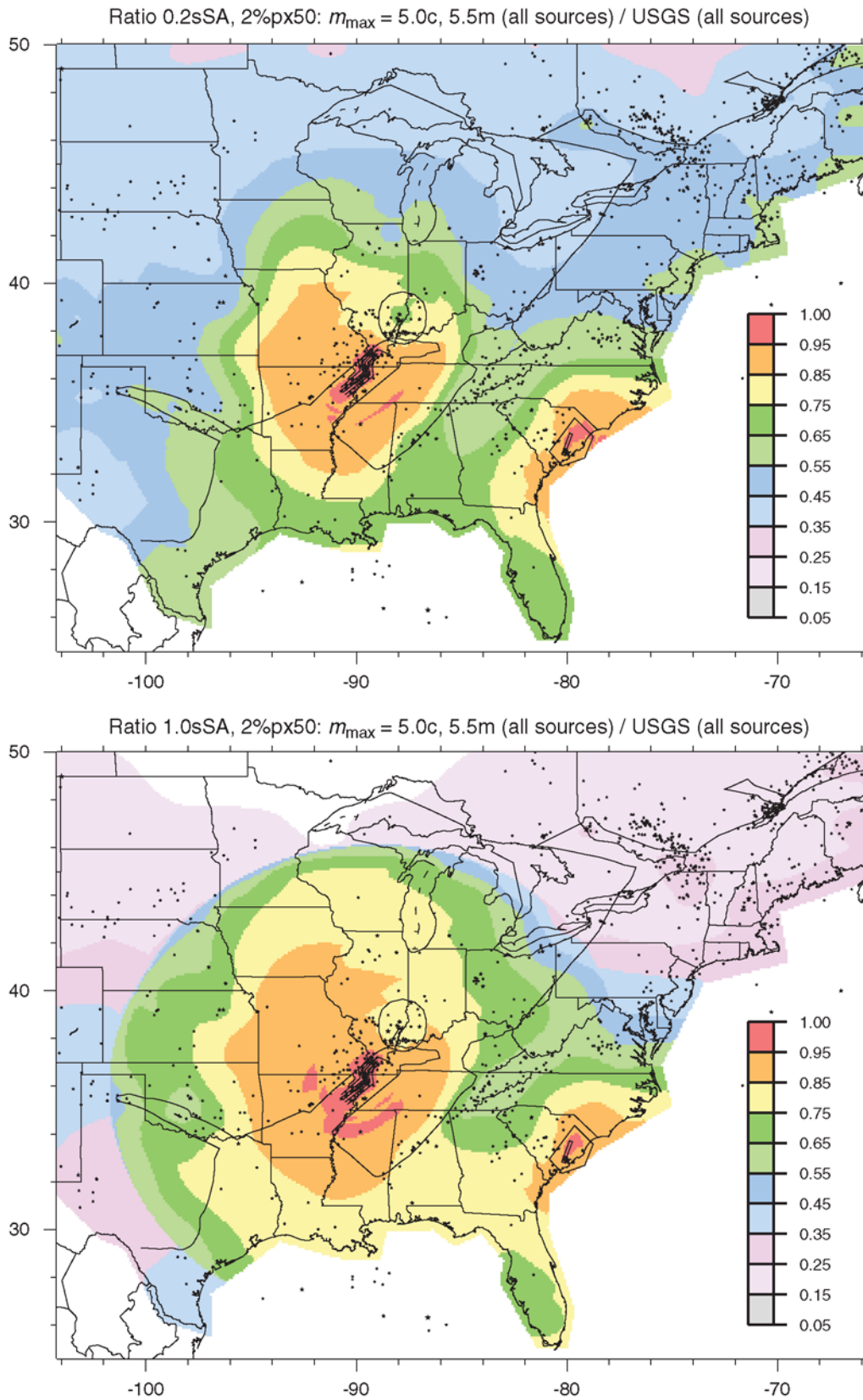


Figure 4. Like Figure 2 but with fault sources added to both the numerator and denominator hazard models. The effect of the m_{\max} truncation for seismicity-based sources is tempered at sites where faults dominate the hazard. Additional black lines show modeled faults and fault zones (see Fig. 1).

Table 6
Hazard Ratios for 10%px50 (about 0.002apx): Alternative m_{\max} (sso)/USGS (sso)

	m_{\max} Model					
	M5.0c5.5m		M6.0c6.5m		M7.0c7.5m	
	0.2sSA	1.0sSA	0.2sSA	1.0sSA	0.2sSA	1.0sSA
Boston	0.58	0.30	0.83	0.63	1.01	1.02
New York City	0.58	0.32	0.84	0.65	1.01	1.02
Washington, DC	0.57	0.29	0.83	0.62	1.01	1.02
Pittsburgh	0.45	0.23	0.76	0.57	1.01	1.02
Charleston	0.61	0.38	0.87	0.71	1.01	1.02
Atlanta	0.55	0.28	0.81	0.63	1.01	1.02
Cincinnati	0.42	0.22	0.75	0.57	1.01	1.02
Chicago	0.37	0.20	0.73	0.56	1.01	1.02
Memphis	0.52	0.28	0.80	0.63	1.01	1.02
Baton Rouge	0.57	0.30	0.82	0.62	1.01	1.02
St. Louis	0.42	0.23	0.75	0.59	1.01	1.02
Minneapolis	0.35	-	0.74	0.55	1.01	1.01
Wichita	0.38	-	0.75	0.55	1.01	1.01
Austin	0.50	-	0.81	0.63	1.01	1.01
Rapid City	0.38	0.20	0.75	0.55	1.01	1.01
Denver	0.42	0.23	0.76	0.57	1.00	1.01

Table 5) and 0.50–0.65 for 1.0sSA (bottom panel of Fig. 3; average hazard ratio about 0.56 ± 0.05 for the 16 cities in Table 5) at most sites. M7.0c7.5m specifies m_{\max} similar to the standard USGS model, lacking only the distributions about the preferred values. Because probabilistic motions change (increase) less than 5%, hazard ratios are not mapped, but values for the 16 cities are listed in Table 5. For M7.5c8.0m, hazard ratios increase to about 1.10–1.20 for 0.2sSA and 1.15–1.40 for 1.0sSA (results not mapped or tabulated).

For the ratio seismic hazard maps shown in Figure 4, M5.0c5.5m again specifies m_{\max} for the seismicity-based sources in the numerator, but now the CEUS faults are added to both the numerator and denominator models. As expected, the effect of the m_{\max} truncation on the hazard is diluted at

sites where the faults make a significant contribution (compare Figs. 4 and 2). In some sense, these results provide a clearer picture of the overall influence of m_{\max} for a realistic PSHA; this point is revisited in the Summary and Discussion section.

Results for Other Probability Levels

Two percent probability of exceedance in 50 years corresponds to an annualized exceedance probability of about 0.0004 (0.0004apx). Results for three other probability levels for the 16 city sites are shown in Tables 6–8: Table 6 for 10% probability of exceedance in 50 years (10%px50, or about 0.002apx), Table 7 for 0.0001 annual exceedance probability (0.0001apx), and Table 8 for 0.00001 annual exceedance

Table 7
Hazard Ratios for 0.0001apx: Alternative m_{\max} (sso)/USGS (sso)

	m_{\max} Model					
	M5.0c5.5m		M6.0c6.5m		M7.0c7.5m	
	0.2sSA	1.0sSA	0.2sSA	1.0sSA	0.2sSA	1.0sSA
Boston	0.53	0.28	0.77	0.58	1.01	1.02
New York City	0.55	0.29	0.79	0.61	1.01	1.02
Washington, DC	0.47	0.23	0.72	0.55	1.02	1.03
Pittsburgh	0.46	0.20	0.72	0.51	1.01	1.02
Charleston	0.54	0.29	0.78	0.61	1.01	1.02
Atlanta	0.45	0.21	0.70	0.53	1.02	1.03
Cincinnati	0.37	0.16	0.68	0.48	1.01	1.02
Chicago	0.40	0.17	0.76	0.51	1.00	1.01
Memphis	0.51	0.23	0.75	0.55	1.01	1.02
Baton Rouge	0.55	0.32	0.80	0.61	1.01	1.02
St. Louis	0.39	0.17	0.73	0.49	1.01	1.01
Minneapolis	0.38	0.15	0.72	0.47	1.00	1.01
Wichita	0.37	0.17	0.73	0.49	1.00	1.01
Austin	0.45	0.23	0.74	0.55	1.01	1.02
Rapid City	0.38	0.19	0.72	0.49	1.00	1.00
Denver	0.40	0.27	0.73	0.52	1.00	1.00

Table 8
Hazard ratios for 0.00001apx: Alternative m_{\max} (sso)/USGS (sso)

	m_{\max} Model					
	M5.0c5.5m		M6.0c6.5m		M7.0c7.5m	
	0.2sSA	1.0sSA	0.2sSA	1.0sSA	0.2sSA	1.0sSA
Boston	0.48	0.24	0.71	0.51	1.02	1.03
New York City	0.49	0.22	0.72	0.52	1.02	1.03
Washington, DC	0.47	0.21	0.71	0.51	1.02	1.03
Pittsburgh	0.50	0.21	0.74	0.51	1.01	1.02
Charleston	0.49	0.22	0.72	0.51	1.02	1.03
Atlanta	0.46	0.19	0.69	0.49	1.02	1.03
Cincinnati	0.38	0.14	0.69	0.45	1.00	1.01
Chicago	0.41	0.16	0.72	0.48	1.00	1.01
Memphis	0.48	0.20	0.71	0.49	1.02	1.03
Baton Rouge	0.52	0.29	0.76	0.57	1.01	1.03
St. Louis	0.40	0.14	0.70	0.45	1.00	1.01
Minneapolis	0.38	0.14	0.71	0.46	1.00	1.00
Wichita	0.40	0.16	0.73	0.48	1.00	1.00
Austin	0.40	0.20	0.69	0.50	1.01	1.02
Rapid City	0.40	0.17	0.71	0.46	1.00	1.00
Denver	0.39	0.26	0.69	0.47	1.00	1.00

probability (0.00001apx). Compared to 0.0004apx, for both models M5.0c5.5m and M6.0c6.5m, hazard ratios at most sites increase 0–15% for 0.002apx, decrease 0–10% for 0.0001apx, and decrease 5–25% for 0.00001apx. In each listed range, smaller and larger numbers generally correspond to the probability-level sensitivities for 0.2sSA and 1.0sSA, respectively. Hazard contributions from seismicity-based sources often shift toward larger, less frequent earthquakes with decreasing probability, and this shift is often stronger for longer structural periods, accounting for the greater m_{\max} effect there. Individual sites can show greater or smaller changes, or even changes that contradict the overall trends: for example, for M5.0c5.5m and 0.2sSA, the hazard ratio decreases about 8% for 0.002apx at Minneapolis, increases about 8% for 0.0001apx at Chicago, and increases about 11% for 0.00001apx at Pittsburgh. Again, these complexities depend on local interactions between the m_{\max} truncation and hazard-controlling earthquakes.

Summary and Discussion

Clearly, some of the discrepancies between USGS and EPRI/SOG-based seismic-hazard estimates that have been seen in recent comparisons can be explained by m_{\max} modeling differences. The smallest- m_{\max} alternative model tested here specifies m_{\max} equal to moment magnitude 5.0 for the craton and 5.5 for the margin, similar to EPRI/SOG for some quiet sources (e.g., Table 2) but much smaller than USGS m_{\max} . The severe m_{\max} truncation has a strong effect, producing hazard ratios equal to 0.35–0.60 for 0.2sSA and 0.15–0.35 for 1.0sSA relative to the USGS model for 0.0004apx (Fig. 2 and Table 5; corresponding to hazard-reduction factors of about 2–3 for 0.2sSA and 3–5 for 1.0sSA). A less truncated model specifies m_{\max} equal to moment magnitude 6.0 for the craton and 6.5 for the margin, similar to EPRI/SOG

m_{\max} for some, more active sources (e.g., Table 1). The milder truncation gives a smaller effect, producing hazard ratios equal to 0.70–0.85 for 0.2sSA and 0.50–0.65 for 1.0sSA relative to the USGS model for 0.0004apx (Fig. 3 and Table 5; corresponding to hazard-reduction factors of about 1.2–1.3 for 0.2sSA and 1.5–2.0 for 1.0sSA). Dependence on probability level is relatively weak. Compared to 0.0004apx, the influence of m_{\max} decreases 0–15% for 0.002apx (that is, hazard ratios are 0–15% greater), increases 0–10% for 0.0001apx (hazard ratios 0–10% smaller), and increases 5–25% for 0.00001apx (hazard ratios 5–25% smaller). Smaller and larger numbers in each listed range generally correspond to the probability-level sensitivities for 0.2sSA and 1.0sSA, respectively.

In practice, the results for M5.0c5.5m would apply to sites where the hazard is dominated by low-activity-rate, seismicity-based sources (Fig. 1). The influence of m_{\max} diminishes in more seismically active regions and where the hazard is dominated by faults, but one example is interesting in this context. The Vogtle nuclear power plant is located near the Savannah River in eastern Georgia, and the EPRI/SOG PSHA for the Vogtle site has been updated for an NRC application (Southern Nuclear Operating Company, 2008). Deaggregations show that for the modeled high-frequency (average 5 and 10 Hz) hazard at Vogtle, the Charleston earthquake (fault) source at a distance of about 130 km is a significant contributor at 0.00001 annual probability of exceedance and dominates at 0.0001 (Southern Nuclear Operating Company, 2008). In determining the high-frequency mean magnitude and distance values in the seismic design analysis, however, seismicity-based sources closer than 105 km from the site (with their corresponding m_{\max} specifications) were considered. In this case, m_{\max} influenced the seismic design, even though seismicity-based sources did not control the hazard.

Model M7.0c7.5m corresponds to the m_{\max} model used in the USGS 2002 National Seismic Hazard Maps (Frankel *et al.*, 2002). Table 5 shows that the expansion into an m_{\max} distribution in the USGS 2008 hazard model (Petersen *et al.*, 2008) has only a small effect on the hazard.

It is not my goal to judge or suggest preferred values for m_{\max} in this study. I would be remiss, however, not to mention one case where the robustness of the EPRI/SOG m_{\max} choices has been challenged by recent data. Table 2 shows that the EPRI/SOG teams specified m_{\max} distributions ranging as small as m_b 4.6 for the host source zones for the South Texas Project nuclear power plant site. In 2006, two earthquakes with magnitudes m_b 5.5 and m_b 6.1 occurred in the Gulf of Mexico. In updating the PSHA (South Texas Project Nuclear Operating Company, 2008), the NRC required the applicant to adjust the m_{\max} distributions for five of the six EPRI/SOG teams upward to accommodate these earthquakes. Even with the updates, at 0.0001 annual exceedance probability, the USGS 10-Hz ground motions exceed the applicant ground motions by factors of two or more.

Data and Resources

No data were used in this study. The web site of the USGS National Seismic Hazard Mapping Project provides links to documentation and software for the 2008 map update (<http://earthquake.usgs.gov/hazards/>, last accessed 13 November 2009). Wheeler (2009) has recently summarized current thinking about best practices for modeling m_{\max} in the CEUS. The figures in this article were made with the Generic Mapping Tools software (Wessel and Smith, 1991).

Acknowledgments

I gratefully acknowledge advice and encouragement from Rus Wheeler and Art Frankel and reviews from Rus Wheeler, Art Frankel, Steve Harmsen, Dave Perkins, Oliver Boyd, John Adams, Chris Cramer, and Martin Chapman. This work was supported by the U. S. Nuclear Regulatory Commission. The PSHA models and computer codes used here were developed by the members of the USGS National Seismic Hazard Mapping Project; Art Frankel and Steve Harmsen deserve special mention.

References

- Atkinson, G. M., and D. M. Boore (1995). Ground motion relations for eastern North America, *Bull. Seismol. Soc. Am.* **85**, 17–30.
- Coppersmith, K. J., A. C. Johnston, A. G. Metzger, and W. J. Arabasz (1987). Methods for assessing maximum earthquakes in the central and eastern United States, *Working Report, EPRI Research Project 2556-12*, Electric Power Research Institute, Palo Alto, California, 137 pp.
- Dominion Nuclear North Anna (2006). Rev. 9 to North Anna Early Site Permit Application (<http://adamswebsearch2.nrc.gov/idmws/ViewDocByAccession.asp?AccessionNumber=ML062580096>, last accessed 22 May 2008).
- Electric Power Research Institute/Seismicity Owners Group (EPRI/SOG) (1988). Seismic hazard methodology for the central and eastern United States, *Final Report for Project NP-4726-A*, Volumes **1–10**, Electric Power Research Institute, Palo Alto, California.
- Felzer, K. R. (2008). Calculating California seismicity rates, in *The Uniform California Earthquake Rupture Forecast, Version 2 (UCERF 2)*, Appendix I, U.S. Geological Survey Open-File Report 2007-1437I and California Geological Survey Special Report 203I, 42 pages.
- Frankel, A. (1995). Mapping seismic hazard in the central and eastern United States, *Seismol. Res. Lett.* **66**, 8–21.
- Frankel, A., C. Mueller, T. Barnhard, D. Perkins, E. V. Leyendecker, N. Dickman, S. Hanson, and M. Hopper (1996). National Seismic Hazard Maps: Documentation June 1996, *USGS Open-File Report 96-532*, 70 pages.
- Frankel, A. D., M. D. Petersen, C. S. Mueller, K. M. Haller, R. L. Wheeler, E. V. Leyendecker, R. L. Wesson, S. C. Harmsen, C. H. Cramer, D. M. Perkins, and K. S. Rukstales (2002). Documentation for the 2002 update of the National Seismic Hazard Maps, *USGS Open-File Report 2002-420*, 39 pages.
- Johnston, A. C. (1994). Seismotectonic interpretations and conclusions from the stable continental region seismicity database, in *The Earthquakes of Stable Continental Regions, V. 1—Assessment of Large Earthquake Potential*, J. F. Schneider (Editor), Electric Power Research Institute, Palo Alto, California, 4-1–4-103.
- Johnston, A. C. (1996). Seismic moment assessment of earthquakes in stable continental regions—I. Instrumental seismicity, *Geophys. J. Int.* **126**, 381–414.
- Mueller, C., M. Hopper, and A. Frankel (1997). Preparation of earthquake catalogs for the National Seismic Hazard Maps—Contiguous 48 states, *U.S. Geological Survey Open-File Report 97-64*, 36 p.
- Petersen, M. D., A. D. Frankel, S. C. Harmsen, C. S. Mueller, K. M. Haller, R. L. Wheeler, R. L. Wesson, Y. Zeng, O. S. Boyd, D. M. Perkins, N. Luco, E. H. Field, C. J. Wills, and K. S. Rukstales (2008). Documentation for the 2008 update of the United States National Seismic Hazard Maps, *U.S. Geological Survey Open-File Report 2008-1128*, 60 pages plus appendixes.
- South Texas Project Nuclear Operating Company (2008). South Texas Project Units 3 & 4 COLA (FSAR), Rev. 1 (<http://adamswebsearch2.nrc.gov/idmws/ViewDocByAccession.asp?AccessionNumber=ML080700763>, last accessed 22 May 2008).
- Southern Nuclear Operating Company (2008). Vogtle Early Site Permit Application, Revision 4, (<http://adamswebsearch2.nrc.gov/idmws/ViewDocByAccession.asp?AccessionNumber=ML081020073>, last accessed 22 May 2008).
- Weichert, D. H. (1980). Estimation of the earthquake recurrence parameters for unequal observation periods for different magnitudes, *Bull. Seismol. Soc. Am.* **70**, 1337–1356.
- Wessel, P., and W. H. F. Smith (1991). Free software helps map and display data, *EOS Trans. AGU* **72**, no. 41, 441, 445–446.
- Wheeler, R. L. (2009). Methods of M_{\max} estimation east of the Rocky Mountains, *U.S. Geological Survey Open-File Report 2009-1018* (online only), 44 pages, (<http://pubs.er.usgs.gov/usgspubs/ofr/ofr20091018>, last accessed 15 September 2009).
- Wheeler, R. L., and C. H. Cramer (2002). Updated seismic hazard in the southern Illinois basin: Geological and geophysical foundations for use in the 2002 USGS National Seismic Hazard Maps, *Seismol. Res. Lett.* **73**, 776–791.
- Wheeler, R. L., and A. Frankel (2000). Geology in the 1996 USGS seismic-hazard maps, central and eastern United States, *Seismol. Res. Lett.* **71**, 273–282.
- Wheeler, R. L., and A. C. Johnston (2008). $M(\max)$ east of the Rocky Mountains, *Seismol. Res. Lett.* **79**, 349.
- U.S. Geological Survey
Mail Stop 966, PO Box 25046
Denver, Colorado 80225
cmueller@usgs.gov